



HAL
open science

A feedback mechanism between crystals and bubbles in a RuO₂-bearing melt

Luiz Pereira, Rafael Nuernberg, Olivier Podda, Norma Machado, Annabelle Laplace, Franck Pigeonneau, Ulrich Kueppers, Kai-Uwe Hess, Donald Dingwell

► **To cite this version:**

Luiz Pereira, Rafael Nuernberg, Olivier Podda, Norma Machado, Annabelle Laplace, et al.. A feedback mechanism between crystals and bubbles in a RuO₂-bearing melt. *Journal of Non-Crystalline Solids*, 2022, 582, pp.121456. 10.1016/j.jnoncrysol.2022.121456 . hal-03928794

HAL Id: hal-03928794

<https://minesparis-psl.hal.science/hal-03928794>

Submitted on 7 Jan 2023

HAL is a multi-disciplinary open access archive for the deposit and dissemination of scientific research documents, whether they are published or not. The documents may come from teaching and research institutions in France or abroad, or from public or private research centers.

L'archive ouverte pluridisciplinaire **HAL**, est destinée au dépôt et à la diffusion de documents scientifiques de niveau recherche, publiés ou non, émanant des établissements d'enseignement et de recherche français ou étrangers, des laboratoires publics ou privés.

A Feedback Mechanism Between Crystals and Bubbles in a RuO₂-Bearing Melt

Luiz Pereira,^{1,2,3*} Rafael Nuernberg,² Olivier Podda,² Norma Machado,² Annabelle Laplace,²
Franck Pigeonneau,³ Ulrich Kueppers,¹ Kai-Uwe Hess,¹ Donald B. Dingwell.¹

¹ Department of Earth and Environmental Sciences, Ludwig-Maximilians-Universität München, Theresienstraße 41, 80333 Munich, Germany.

² CEA, DES, ISEC, DE2D, Univ Montpellier, Laboratoire de Développement des Matrices de Conditionnement, Marcoule, France.

³ Centre for Material Forming, CEMEF, MINES ParisTech, PSL Research University, CNRS UMR 7635, CS 10207, Claude Daunesse, 06904, Sophia Antipolis Cedex, France.

* luiz.pereira@min.uni-muenchen.de

ABSTRACT

Crystals are known to affect bubble behavior in both natural and industrial glass melts. In volcanic systems, high crystal contents ($\phi_c > 30$ vol.%) may drastically increase the suspension viscosity, altering bubble dynamics severely enough to modify eruptive style. During industrial glass production, the presence of crystals can corrupt the process and the final product. In this present work, we investigate how a small crystal fraction of nano-sized RuO₂ ($\phi_c \sim 2.0$ vol.%, *i.e.* 5.0 wt.%) modifies bubble behavior in a molten glass, generating a cyclic gas-release phenomenon. We conduct a series of high-temperature, lab-scale, crucible tests, on a three-phase system composed of a Ce-bearing borosilicate melt, bubbles, and RuO₂ crystals. Optical microscopic investigation is performed on the products of thermal treatment at 1000 °C (in air and without

agitation) for different dwell times. Based on viscosity measurements on the crystal-bearing melt, contact angle measurements in the melt-RuO₂-air system, and numerical simulations of bubble-crystal attachment, we propose a mechanism of entrainment of bubbles carrying crystals to the upper free surface accompanied by crystal aggregation, and followed by an increase in viscosity to explain the phenomenon of cyclic gas-release observed in this system.

KEYWORDS: melt, bubbles, crystals, crystal flotation, crystal aggregation, outgassing.

1. INTRODUCTION

The bubble behavior in melts is well-studied topic in both glass science and earth sciences. In the former, bubbles may impact both the glass-melting process and the final product.(1) In the latter, bubble dynamics is an important parameter dictating on whether an eruption will be effusive or explosive.(2) Bubbles affect different properties of silicate melt bodies, such as bulk viscosity, density, and electrical conductivity.(2, 3) Conversely, silicate melt properties, such as viscosity, dissolved gases, and the presence of crystals may influence bubble dynamics.(4-6) These solid crystalline inclusions can be found in melts in both in industry and in nature. In nuclear waste vitrification at high-temperature, platinum group element particles are common due to their poor solubility (7). In magmatic processes, predominantly silicate crystals are generally formed from crystallization of the parental melt during cooling.(8)

Crystals can affect several properties of bubble-bearing melts. The presence of crystals may drastically increase the suspension viscosity.(6, 9) Likewise, it has been shown that crystals affect the electrical properties of silicate melts and glasses.(10, 11) Finally, crystals may also influence bubble behavior in molten glasses. Physical interactions between bubbles and crystals affect gas migration and, in volcanological processes, it may play an important role in eruption dynamics of crystal-rich magmas.(12) In Strombolian-type eruptions, the transition between effusive to explosive styles may be related to several features of the crystalline phase.(12-14) Analogue experiments at room temperature containing micro-sized particles have demonstrated that at low particle concentrations ($\phi_c < 30$ vol.%), small bubbles could rise steadily through the conduit and accumulation of coalesced bubbles (slugs) at the top surface is not been observed. However, at higher crystal concentrations ($\phi_c > 30$ vol.%), a slug could be formed due to the obstruction created by the crystal-rich plug on the top layer of the volcanic conduit.(13, 14) This critical crystallinity of ~ 30 vol.% can lock up magmas and trigger explosions even for basaltic magmas.(6, 15) Di Genova et al.(15) have recently illustrated how a small fraction of nanocrystals

can cause a disproportional increase in magma viscosity, locking up the free surface and causing explosions.

Given these analyses of the influence of crystal content on the behavior of bubbly melts, here we focus on understanding how RuO₂ crystals might affect bubble behavior in a borosilicate melt system at high-temperature (borosilicate melt being relevant to nuclear waste immobilization). RuO₂ is known to be sparingly soluble in oxide glasses.⁽¹⁶⁾ Here, a series of experiments were performed on a three-phase system composed of a Ce-bearing borosilicate melt, bubbles, and RuO₂ crystals.⁽¹⁶⁻¹⁸⁾ A postmortem optical microscope analysis was performed to document bubble kinematics in the solidified samples after thermal treatments at 1000 °C for different dwell times. Our experiments were carried out in air without forced convection. Additionally, viscosity measurements on the crystal-rich melt and contact angle measurements on melt-RuO₂-air system were carried out to help constrain the observed behavior. Finally, theoretical calculations on bubble-crystal surface interaction were performed with the purpose of identifying controlling phenomena. In doing so we hope to shed light on why small concentrations ($\phi_c \sim 2.0$ vol.%, *i.e.* 5.0 wt.%) of RuO₂ crystals play a determining role on bubble behavior in this system.

2. MATERIALS AND METHODS

2.1 High-temperature synthesis

To study the interaction of ruthenium oxide crystals with a bubble-bearing melt, we prepared different samples by mixing borosilicate glass powder (250 – 500 μm), previously synthesized at 1450 °C, together with 0.1 wt.% CeO₂ powder (< 5 μm , >99.9%, Aldrich) and with 5.0 wt.% (1.98 vol.%) RuO₂ powder (> 99.9%, Heraeus). The borosilicate glass composition has been presented previously.⁽¹⁹⁾ The particle size distribution (PSD) of RuO₂ is displayed in Figure 1.⁽¹⁰⁾ It can be seen that (despite the presence of a peak in the micrometric region in the ‘volume (%)’ plot) the vast majority of particles are nanoparticles. At 1000 °C, the borosilicate liquid has

a viscosity and a density of 74.34 Pa.s and 2283.3 Kg/m³, respectively.(19) The surface tension between an oxygen bubble and the borosilicate liquid is 0.2498 N/m.(19) Ruthenium oxide has density of 6970 Kg/m³, and due to its very low solubility (hundreds of ppm), most is present as RuO₂ nanocrystals (polyhedral shapes).(16)

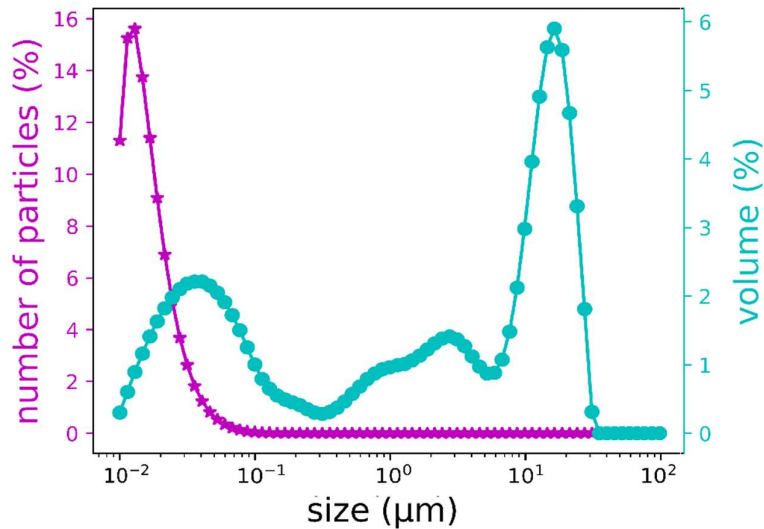


Figure 1: Distribution of the percentage of the number of RuO₂ particles (magenta stars) and the distribution of the percentage of the volume of RuO₂ particles (cyan circles).

For each sample, 20 g of material was synthesized according to the following procedure. The borosilicate, the CeO₂, and the RuO₂ powders were mixed mechanically and then placed in cylindrical alumina crucible (CeraQuest AC20 material AF997) with an outer diameter, a height, and wall thickness equal to 30, 40, and 2 mm respectively. This assembly was loaded into a hot furnace (1000 °C) and melted in air and with no external agitation at this same temperature for different dwell times (20, 30, 40, 60, 80, 100, and 120 min). The samples were subsequently removed from the furnace and cooled in air. They were filled with epoxy resin and subsequently cut into two halves for microscopic investigation.

2.2 Optical-Laser Microscopy postmortem analysis

A KEYENCE Confocal Optical-Laser Microscope (VK X-1000 Series) was used to assemble an entire cross-sectional area of the samples using mapping techniques. This procedure assembles 144 images overlapping to generate the surface. The acquired images have a resolution of 1.85 pixel/ μm and they were treated using NIH (National Institute of Health) software to yield an inventory of bubbles with their diameters as well as information on RuO_2 crystals.

2.3 Rheological measurements

Rheological measurements were carried out using Rheometrics Scientific SR5000, in which the characterization cell is placed into a vertical tubular furnace. The cell is a platinum-rhodium crucible (27 mm diameter, 40 mm length) placed at the center of the furnace and the geometry used is a multiblade rotor (18 mm diameter, 27 mm length). This equipment is discussed in more detail elsewhere.(20)

The studied samples were firstly synthesized at 1000 °C during 360 min in isotherm furnace in air (no cold cap) to eliminate bubbles and obtain a two-phase system (RuO_2 + borosilicate liquid). Subsequently, the system was submitted to a pre-sheared situation (shear rate, $\dot{\gamma} = 40\text{s}^{-1}$ during 60 s) in the rheometer to disperse RuO_2 particles in the melt.(9) Viscosity measurements were conducted over ca. two hours at two distinct shear rate values for molten glass systems containing RuO_2 crystals ($\dot{\gamma} = 0.02$ and 1.50 s^{-1}). (9) The recorded viscosity were obtained in the steady-state regime.

2.4 Bubble- RuO_2 contact angle

The contact angle (Ψ) between bubbles and a RuO_2 substrate immersed in the borosilicate melt was measured. First, a parallelepiped sample ($8 \times 8 \times 3\text{ mm}^3$) of metallic ruthenium (Goodfellow, 99.9%) was polished ($R_a = 0.752 + 0.05\text{ }\mu\text{m}$). Subsequently, following the protocol proposed in

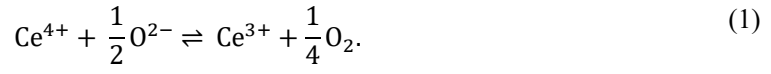
Coloma-Ribera et al.,(21) the metallic ruthenium sample was oxidized in air at 400 °C during 108 h to obtain a dense and homogeneous RuO₂ layer. Scanning electron microscopy coupled with energy dispersive X-ray (Hitachi SU5000 with working conditions of 20 kV, 0.15 mA, and 10.3 mm working distance) was used to confirm that a RuO₂ layer (~ 0.1 μm thick) had been formed across the surface of the sample.

This sample was placed at the bottom of an alumina crucible, covered with borosilicate glass powder and placed in a pre-heated furnace (at 1000 °C, air atmosphere) for ~ 10 min. These resultant samples were then submitted to a series of cutting and polishing procedures to access the interface in which bubbles were attached to the RuO₂ surface. Finally, this bubble-RuO₂ interface was analyzed via optical microscopy and the contact angles (averaging 10 measurements) were obtained via image analysis (Fig. S1 in the supplementary material).

3. RESULTS AND DISCUSSION

3.1 Bubble formation

As demonstrated previously, bubbles in this type of system are formed from pre-existing trapped air bubbles.(4) Indeed, granular media generally yield bubbles formed from air-entrapment when subjected to a high heating rate.(4, 22) The presence of crystals does not affect this type of bubble formation strongly, as no nucleation is required. These bubbles initially contain air via entrapment during melting of the glass beads and are subsequently the sink for oxygen gas produced by the reduction of cerium in the melt (Eq. 1). Initially, the bubbles are homogeneously distributed in the crucible(4). Similarly, due to the mechanical mixing of the powders before the melting step, RuO₂ crystals are also initially homogeneously dispersed in the melt phase.



3.2 Bubble dynamics

Figure 2 shows optical microscope images of the three-phase system synthesized at 1000 °C for different time durations (20, 30, 40, 60, 80, 100, and 120 min). The assembly of these images gives an overview of size and spatial distribution of bubbles and crystals. It is important to emphasize that this study was done using seven different samples in total and the images do not represent a temporal evolution of a single experiment. It is apparent that some bubbles are attached to RuO₂ crystals, indicating an interaction between these two phases. Such crystal-bubble attachments may help explain the presence of RuO₂ crystals at the top surface of the melt in the crucible, despite having a density (6970 Kg/m³) three times higher than the melt phase (2283 Kg/m³).⁽¹⁹⁾ Further, despite the nanometric initial size of the RuO₂ precursor (Figure 1), it can be found as large micrometric clusters or aggregates.^(9, 10)

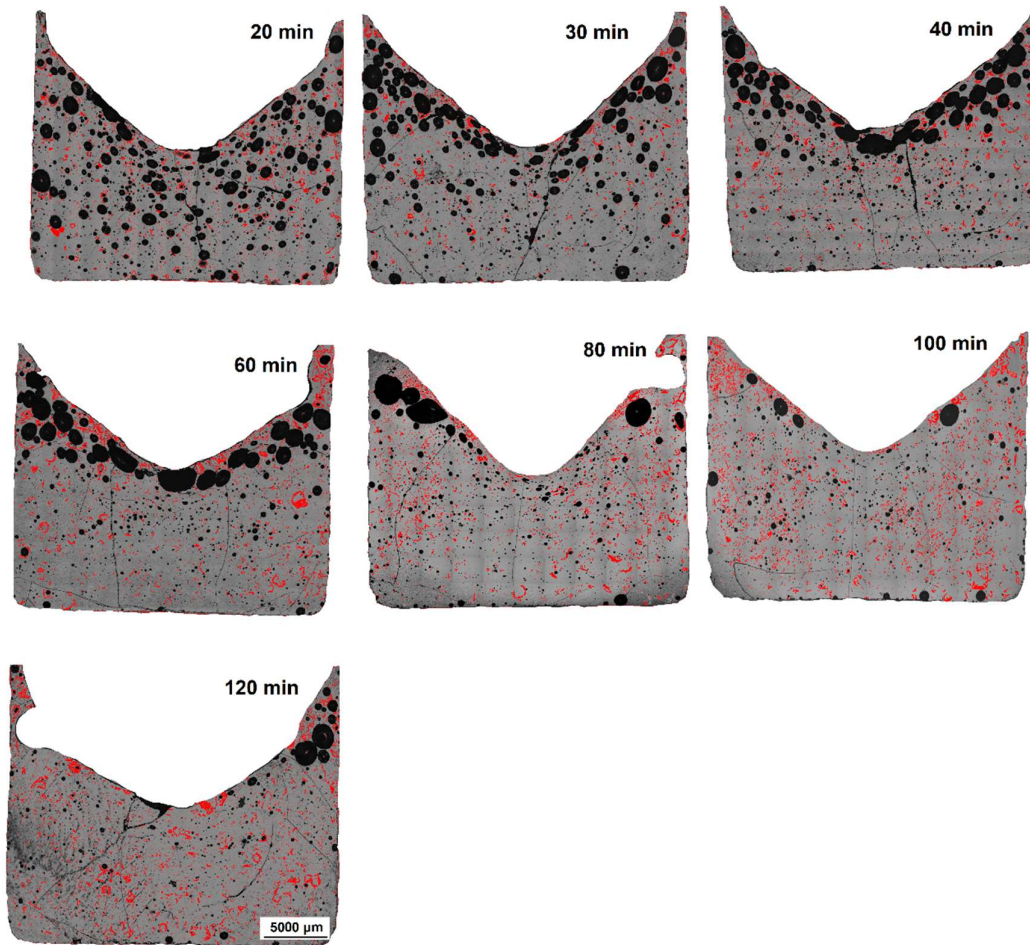


Figure 2: Optical microscope images of samples containing the borosilicate melt (grey), RuO₂ (red), and bubbles (black) prepared at 1000 °C for different dwell times.

These bubble-crystal attachments together with crystal aggregation likely contribute as well to the genesis of a crystal-rich plug at the top layer of the crucible. Figure 3 depicts a left-corner zoom of the image shown in Figure 2 (after 80 min) and illustrates this crystal aggregation at the top layer. This crystal-plug, due to its higher overall viscosity, hinders gas percolation through the system, generating bubble accumulation at the free surface. Figure 4 exhibits the relative bubble fraction ($\phi_b/\phi_{b(\text{total})}$) at different heights in the crucible (H) for two samples. It can be seen that in the early stages (sample 1000 °C - 20 min), there is a roughly homogenous distribution of bubbles throughout the crucible. For the sample 1000 °C - 60 min, bubbles are accumulated at the top layer, with a relative bubble fraction of ~ 0.65 . In this latter case, the crystal-rich plug

noted above promotes gas accumulation in pockets, as so-called slugs. Pereira et al.(3, 4) studied an equivalent crystal-free system. There, no bubble accumulation was observed at the free surface of the crucible and bubble dynamics were mainly controlled by the viscosity of the liquid phase.

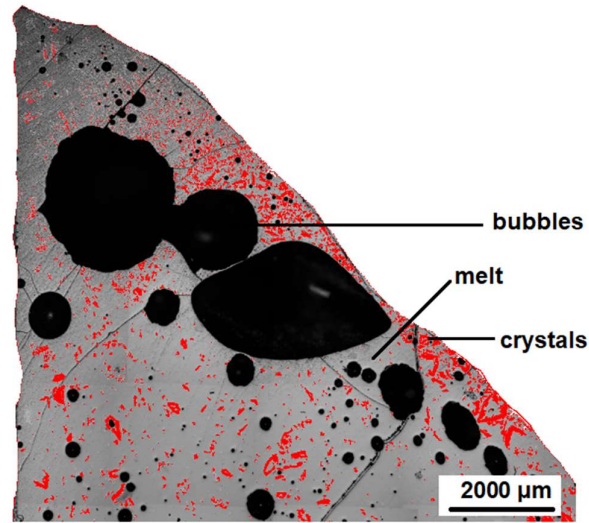


Figure 3: Optical microscope image of the sample 1000 °C - 80 min showing a crystal-rich plug created at the top layer of the crucible due to bubble-crystal attachment and crystal aggregation tendency.

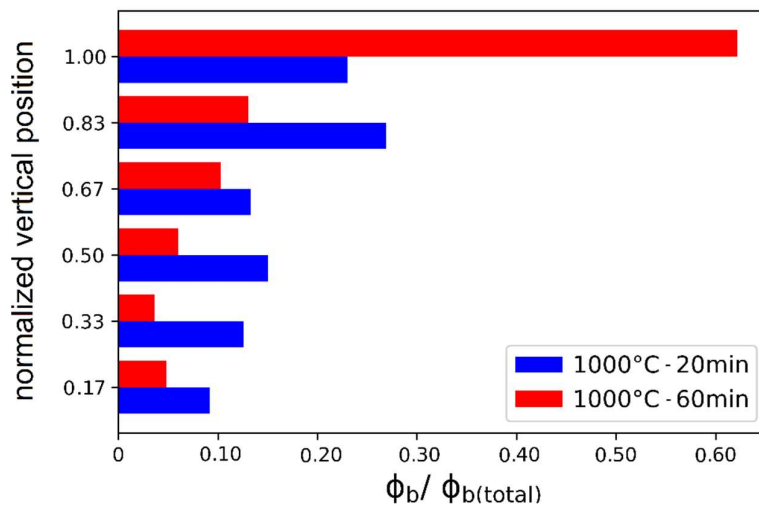


Figure 4: Relative bubble fraction ($\phi_b/\phi_{b(\text{total})}$) for different heights of the crucible for two samples: 1000 °C - 20 min (blue) and 1000 °C - 60 min (red).

Figure 5 displays the mean bubble surface fraction (ϕ_b) as a function of time obtained from the image treatment of the optical microscope images of the studied sample. Two different behaviors are observed. Initially (20 - 40 min), bubbles appear to escape the crucible steadily with time and the bubble fraction decreases continuously (behavior A). Subsequently (40 - 60 min), a crystal-rich plug is formed and an obstruction of bubbles at the upper surface results such that the bubble fraction ceases to decrease (behavior B). Next (60 - 100 min), bubbles appear to leave the crucible steadily again and bubble fraction decreases, repeating 'behavior A'. Finally (100 - 120 min), a few remaining bubbles seem to be impeded from escaping the crucible due to the presence of the few remaining crystals at the free surface (behavior B). It is important to note that, unlike what is observed in volcanic system, there is no continuous gas supply in our laboratory scale tests.

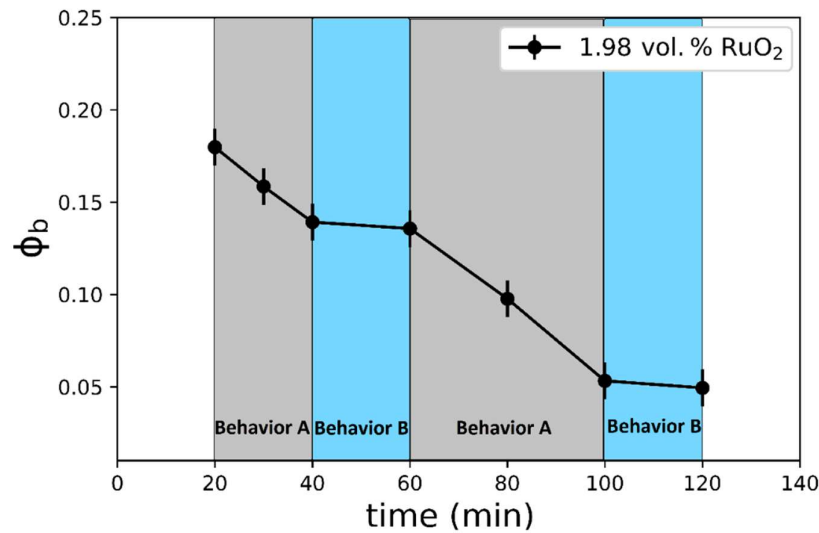


Figure 5: Bubble fraction (ϕ_b) evolution for the samples studied in laboratory scale.

It is interesting nonetheless to recognize the similarity between the bubble behavior in our current three-phase system and the behavior observed at Strombolian-type volcanos, which are composed of a basaltic melt, crystals, and bubbles. As previously mentioned, Strombolian-type eruptions display intermittent explosive periods separated by effusive ones. These natural systems generally contain more than ~ 30 vol.% of crystals, and at this stage a crystal-rich plug is formed.(13) In such a scenario, the cyclic behavior associated with intermittent gas release by bursting of

coalesced bubbles can be observed.(12-14) For our system, this cyclic behavior appears to occur at a much lower crystal fraction (~ 2.0 vol.%). In the following section, we analyze the nature of this cyclic slug-releasing phenomenon at low crystallinity.

3.3 Rheology of RuO₂ melt suspensions

Di Genova et al.(15) have recently investigated a basaltic volcanic system containing nano-sized crystals. They also discussed the critical crystallinity of 30 vol.% for micro-sized crystals, which can lock up magma and trigger explosions. In that study, they showed that, for nanocrystals, this critical crystallinity is reduced due to a disproportional increase in magma viscosity with crystallinity. Investigating analogue magmas composed of nano-sized particles at room temperature, they observed an enormous increment of the system viscosity at volcanologically relevant shear rates. For a shear rate of 1.0 s^{-1} , ~ 65 vol.% of microparticles is required to reach the maximum packing density (ϕ_m), while for nanoparticles the same effect can be produced at just 4.5 vol.%(15) Considering such large purported influences of nano-sized particles on the system rheology, we have attempted to verify for our system if the viscosity increment could be the explanation for the transition between the degassing styles.

Figure 6 exhibits the viscosity measurements on two-phase system containing the Ce-bearing borosilicate melt doped with 1.98 vol.% of RuO₂ crystals. Two shear rate values were selected based on Hanotin et al.(9) to represent two different situations: one above and one below the critical shear rate in which RuO₂ chains are broken. In the first case, at high shear rate (green), the system behaves as a suspension of small clusters and the viscosity is largely controlled by the viscosity of the liquid phase, behaving therefore as a classical suspension. However, at low shear rate (blue), they observed large aggregates made up of chains of RuO₂ particles separated by a thin layer of melt. In the presence of RuO₂ chains, the system viscosity is strongly increased. A thixotropic behavior is observed for this type of crystal-melt composite.(9)

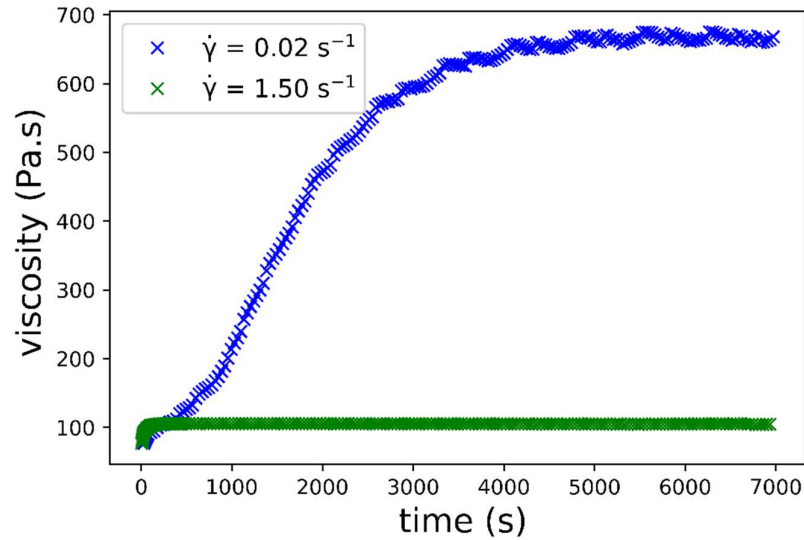


Figure 6: Viscosity measurements on the two-phase system containing the Ce-bearing borosilicate melt and RuO₂ crystals.

To verify if this observed increase in viscosity could be a factor contributing to locking-up of the system and change the bubble dynamics, we compare our data with that of Di Genova et al.(15) for the same crystal fractions, similar sizes, and similar aspect ratios. Figure 7 exhibits the relative viscosity ($\eta/\eta_{\text{liquid}}$) obtained on analogue magma system composed of silicon oil and nano-sized added SiO₂ particles (spherical shape)(15) as well for our current viscosity results on the Ce-bearing borosilicate melt with nano-sized added RuO₂ crystals (polyhedral shape).(16) It can be seen that the increase in viscosity for our system is around eight times the liquid viscosity, whereas for their system, in which the lock-up scenario has been observed, the increase in viscosity is more than sixty times the liquid viscosity. Indeed, the suspension containing 1.98 vol.% of RuO₂ crystals has lower crystallinity than the critical one ($\phi_m = 4.5$ vol.%) calculated in the supplementary material of Di Genova et al.(15) Therefore, the increase in the suspension viscosity does not appear to be sufficient to precipitate the transition between the two behaviors. Despite their being added in nanometric size, the RuO₂ crystals undergo aggregation and are thus generally not present as isolated nano-crystals.(10) This aspect may explain the smaller increase in viscosity when compared to the rheological data from Di Genova et al.(15)

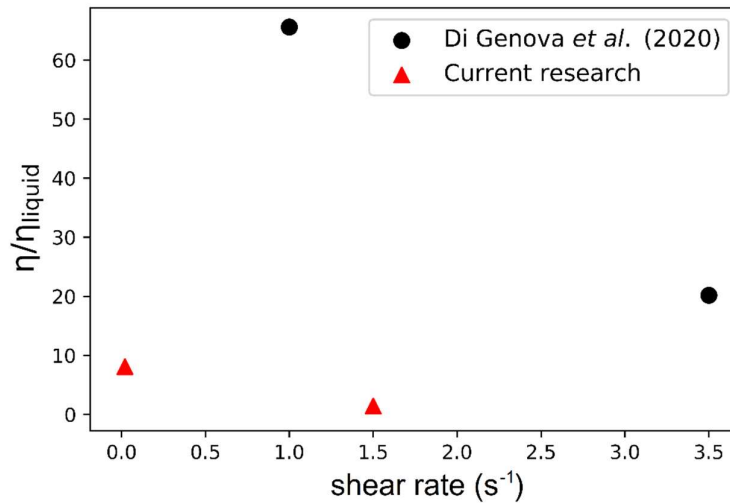


Figure 7: Viscosity measurements of crystal-rich magma at different shear rates from Di Genova et al.(15) and this present work.

3.3.3.4 Bubble-crystal surface interaction

The wettability among different phases is an important feature that may explain the cyclic gas release phenomenon observed for the studied system. The wettability properties of particles in a suspension play a crucial role in bubble-particle attachment. These properties have been extensively investigated in froth flotation science. In this field, bubbles selectively adhere to minerals and carry them to the surface of the system to be collected, while other minerals stay in the aqueous slurry medium.(23) Figure 2 and Figure 3 confirm that, in the investigated system, we can observe bubbles attached to crystals. Gaulda and Ghiorso(24) demonstrated mathematically that the attachment of a bubble to a mineral substrate is always energetically favored. Despite of the RuO₂ density being about three times that of the surrounding melt, these crystals were found at the top surface of the crucible, attached to bubbles. It demonstrates once again that bubbles and crystals may interact well and thus crystals may have reached the free-surface due to bubble-crystal attachment phenomena.

The wettability between different phases is generally expressed by a contact angle (Ψ), which is a direct measurement of the nature of interaction between them.(23) The Ψ is the angle formed

when a gas wets a solid substrate immersed in a liquid. This contact angle, measured for 10 bubbles attached to the RuO₂, is $\Psi = 41.4 \pm 3.5^\circ$. Fig. S1 in the supplementary material shows an example of contact angle measured for our studied sample ($\Psi = 38.4^\circ$). As previously mentioned, for $\Psi > 0$, there may be a bubble-particle attachment.(24) In bubble-mineral-melt systems, the higher the contact angle, the more stable a particle is attached to a bubble and more likely it will be transported to the upper layer of the system.(24) To keep the neutrality buoyant bubble-mineral pair joined, the attachment force (F_{attach}) has to be equal or larger than the separating force due to the difference in buoyancy of bubble and crystal ($\Delta F_{\text{buoyancies}}$). In practical terms, this latter term is proportional to the bubble buoyancy minus the crystal buoyancy. Based on this previous statements, Gaulda and Ghiorso(24) proposed a mathematical model. The attachment force derived from the attachment energy between a spherical crystal and a spherical bubble is presented in Eq. 2 and the difference in buoyancy of crystal and bubble is given in Eq. 3:

$$F_{\text{attach}} = 2\pi R_b \sin^2(180 - \psi) \sigma_{\text{b-mel}} \left[\frac{4}{2 - 3 \cos(180 - \psi) + \cos^3(180 - \psi)} \right]^{\frac{1}{3}}, \quad (2)$$

$$\Delta F_{\text{buoyancie}} = -\frac{4}{3}\pi(R_c)^3(\rho_c - \rho_{\text{melt}}) - \frac{4}{3}\pi(R_b)^3(\rho_b - \rho_{\text{melt}}), \quad (3)$$

where R_b is the bubble radius, $\sigma_{\text{b-mel}}$ is the surface tension of the bubble immersed in the borosilicate melt, R_c is the crystal (or cluster) radius, ρ_c is the crystal density, ρ_{melt} is the melt density, and ρ_b is the gas inclusion density.

We developed a Python script based on this mathematical approach described in Gaulda and Ghiorso(24) and we applied to the studied system by using the bubble size distribution, the crystal-cluster size distribution, and the physical properties of the three-phase system. Figure 8

shows the bubble and crystal-clusters histograms which illustrate their size distributions for the initial sample (1000 °C - 20min). Since bubble radius plays an important role on bubble dynamics and our current experimental method allow us to examine a 2D image, we applied the *GrainSizeTools* Python script to unfold the 2D bubble size distribution into the actual 3D bubble size distribution.(25) This conversion is done based on stereological techniques, more precisely the Saltikov method.(26)

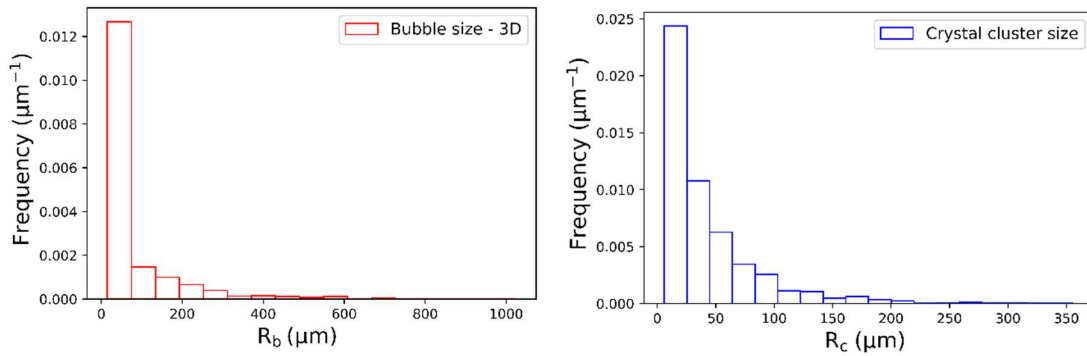


Figure 8: Histogram illustrating the 3D bubble and crystal cluster size distributions for the sample 1000 °C - 20 min.

Figure 9 shows the attachment force balance model applied to the current three-phase system considering the initial conditions at 1000 °C - 20 min. The calculations have been performed considering bubbles and crystals as spheres. Five relevant RuO₂ cluster radii (1, 100, 200, 300, 400 μm) were considered in the calculations. To keep the neutrality buoyant bubble-crystal pair joined, the attachment force has to be equal or larger than the separating forces due to the difference in buoyancies. In the investigated system, the ratio between attachment force over detachment forces increases with bubble radius until a maximum value is reached. After this inflexion point, the large upward force due to the large bubble radii starts to weaken the bubble-crystal pair. By keeping increasing bubble radius, at a given bubble radius ($R_b \sim 2000 \mu\text{m}$) the detachment forces overtake the attachment one; and the bubble-crystal pair is no longer stable. Thus, bubble-crystal attachment for this current system is favorable for most scenarios in terms of bubble and crystal cluster radii. Therefore, at the investigated conditions, bubble-RuO₂

attachment is likely to occur and can explain the crystal accumulation at the top surface, despite the much higher crystal density when compared to its surrounding melt.

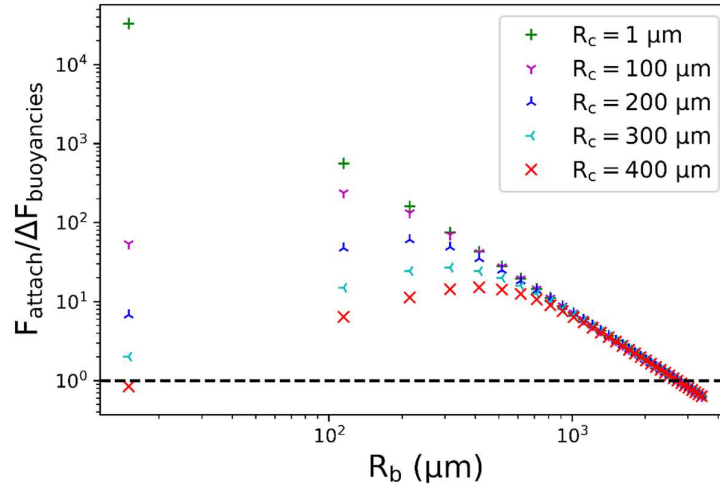


Figure 9: Bubble-crystal attachment force balance model applied to the current three-phase system at initial situation (1000 °C - 20 min) for four different crystal cluster radii.

This phenomenon, observed on laboratory scale, may be compared to fractional crystallization in magmatic systems. It is one of the fundamental mechanisms controlling magma differentiation and ore deposit formation. It results from gravitational settling or floatation of minerals based on their density contrast with the surrounding silicate melt. Less dense minerals (*e.g.*, plagioclases $\sim 2.6 - 2.7 \text{ g.cm}^{-3}$) are separated by mineral floatation, while dense ones (*e.g.*, magnetite $\sim 5.15 \text{ g.cm}^{-3}$, olivines $\sim 3.3 \text{ g.cm}^{-3}$) are separated by gravitational settling. However, in the presence of bubbles, some authors demonstrated that bubble-magnetite pair is likely to happen owing their large wetting angles ($\Psi = 45 - 50^\circ$).^(27, 28) Therefore, due to this interaction, bubble-magnetite pair do ascend in silicate melt, accumulating in the upper layers, similarly to what has been demonstrated in this current research for ruthenium-IV oxide.

4. CONCLUSION

A series of lab-scale crucible tests were performed at 1000 °C for different durations on a three-phase system composed of a Ce-bearing borosilicate melt, bubbles, and RuO₂ crystals. Despite of the low crystallinity of the studied system (~ 2 vol.% *i.e.* 5.0 wt.%), we present evidence supporting the idea of a cyclic gas-releasing phenomenon, similar to one observed in Strombolian-type volcanic systems. In such natural systems, in which the crystals derive from crystallization of the parental melt, this phenomenon takes place, for micrometer-sized crystals, at much higher crystallinities ($\phi_c > 30$ vol.%). Based on the experimental and theoretical approaches presented here, we present a mechanism to explain the bubble-RuO₂ crystal interaction in a borosilicate glass melt at high temperature and how RuO₂ crystals influence bubble dynamics. Based on our experimental data and physical characterization, we conclude that the suspension viscosity containing 1.98 vol.% of RuO₂ is not high enough to lock-up the suspension and cause a transition between styles. However, bubble-crystal surface interaction has been investigated and at the conditions investigated, bubble-RuO₂ attachment is highly probable and likely contributes to crystal accumulation at the top surface. At this top surface, due to the tendency for RuO₂ to aggregate, large clusters are formed. As demonstrated in Hanotin et al.(9) and Puig et al.,(20) the local viscosity of the system may be drastically increased (up to 4 orders or magnitude), hindering bubbles from escaping and consequently creating a bubble accumulation underneath the crystal-rich plug. Bubble accumulation leads to a cyclic growth and destruction of a surface crystal-rich plug followed by its reconstruction and so on, yielding a cyclic gas-release phenomenon.

5. ACKNOWLEDGMENTS

Luiz Pereira thanks the *Commissariat à l'énergie atomique et aux énergies alternatives (CEA)* for the funding support during his PhD and *Ludwig-Maximilians-Universität München* for the provided ERC-GA-834225 post-doctoral grant. Norma Machado and Olivier Podda acknowledge the *Commissariat à l'énergie atomique et aux énergies alternatives (CEA)* for the funding support. Dr. Erika Griesshaber (*Ludwig-Maximilians-Universität München*) is thanked for the support offered in the polishing procedure. We thank Dr. Danilo Di Genova (*Universität*

Bayreuth), Dr. Francisco Cáceres (*Ludwig-Maximilians-Universität München*), and Dr. Carlos Veloso (ArcelorMittal Global R&D Metz) for the fruitful discussions and advice given. D.B. Dingwell acknowledges the support of 2018 ADV Grant 834225 (EAVESDROP).

6. REFERENCES

1. Cable M. A Century of Developments in Glassmelting Research. *Journal of the American Ceramic Society*. 1998;81(5):1083-94.
2. Gonnermann HM, Manga M. Dynamics of magma ascent in the volcanic conduit. In: Lopes RMC, Fagents SA, Gregg TKP, editors. *Modeling Volcanic Processes: The Physics and Mathematics of Volcanism*. Cambridge: Cambridge University Press; 2013. p. 55-84.
3. Pereira L, Neyret M, Laplace A, Pigeonneau F, Nuernberg R. Inferring bubble volume fraction in a glass melt through in situ impedance spectroscopy measurements. *International Journal of Applied Glass Science*. 2021;12(3):358-66.
4. Pereira L, Podda O, Fayard B, Laplace A, Pigeonneau F. Experimental study of bubble formation in a glass-forming liquid doped with cerium oxide. *Journal of the American Ceramic Society*. 2020;103(4):2453-62.
5. Behrens H, Gaillard F. *Geochemical Aspects of Melts: Volatiles and Redox Behavior*. *Elements*. 2006;2(5):275-80.
6. Liu Z, Pandelaers L, Blanpain B, Guo M. Viscosity of Heterogeneous Silicate Melts: A Review. *Metallurgical and Materials Transactions B*. 2018;49(5):2469-86.

7. Gin S, Jollivet P, Tribet M, Peugeot S, Schuller S. Radionuclides containment in nuclear glasses: An overview. *Radiochimica Acta*. 2017;105.
8. Bowen NL. *The evolution of the igneous rocks*. Princeton, New Jersey: Princeton University Press; 1928.
9. Hanotin C, Puig J, Neyret M, Marchal P. Platinum group metal particles aggregation in nuclear glass melts under the effect of temperature. *Journal of Nuclear Materials*. 2016;477.
10. Nuernberg R, Machado NM, Malki M, Neyret M. Electrical behavior of RuO₂-glass composites: The effect of RuO₂ particle size on the percolation threshold. *Journal of Nuclear Materials*. 2021;546:152777.
11. Gaillard F, Iacono-Marziano G. Electrical conductivity of magma in the course of crystallization controlled by their residual liquid composition. *Journal of Geophysical Research*. 2005;110.
12. Oppenheimer J, Capponi A, Cashman K, Lane SJ, Rust AC, James M. Analogue experiments on the rise of large bubbles through a solids-rich suspension: A “weak plug” model for Strombolian eruptions. *Earth and Planetary Science Letters*. 2020;531:115931.
13. Woitischek J, Edmonds M, Woods A. The control of magma crystallinity on the fluctuations in gas composition at open vent basaltic volcanoes. *Scientific Reports*. 2020;10:14862.
14. Spina L, Morgavi D, Costa A, Scheu B, Dingwell D, Perugini D. Gas mobility in rheologically-layered volcanic conduits: The role of decompression rate and crystal content on the ascent dynamics of magmas. *Earth and Planetary Science Letters*. 2019;524.

15. Di Genova D, Brooker R, Mader H, Drewitt J, Longo A, Deubener J, et al. In situ observation of nanolite growth in volcanic melt: A driving force for explosive eruptions. *Science Advances*. 2020;6:1-13.
16. Boucetta H, Podor R, Stievano L, Ravaux J, Carrier X, Casale S, et al. Mechanism of RuO₂ crystallization in borosilicate glass: an original in situ ESEM approach. *Inorg Chem*. 2012;51(6):3478-89.
17. Plodinec J. Borosilicate Glasses for Nuclear Waste Immobilization. *Glass Technology - European Journal of Glass Science and Technology Part A*. 2000;41:186-92.
18. Pinet O, Phalippou J, Nardo C. Modeling the redox equilibrium of the Ce⁴⁺/Ce³⁺ couple in silicate glass by voltammetry. *Journal of Non-crystalline Solids*. 2006;352:5382-90.
19. Pereira L, Kloužek J, Vernerová M, Laplace A, Pigeonneau F. Experimental and numerical investigations of an oxygen single-bubble shrinkage in a borosilicate glass-forming liquid doped with cerium oxide. *Journal of the American Ceramic Society*. 2020;103(12):6736-45.
20. Puig J, Bottelin Hanotin C, Neyret M, Marchal P. High temperature rheological study of borosilicate glasses containing platinum group metal particles by means of a mixer-type rheometer. *Journal of Nuclear Materials*. 2015;469.
21. Coloma Ribera R, Kruijs R, Yakshin A, Bijkerk F. Determination of oxygen diffusion kinetics during thin film ruthenium oxidation. *Journal of Applied Physics*. 2015;118:055303.

22. Jones SF, Evans GM, Galvin KP. Bubble nucleation from gas cavities — a review. *Advances in Colloid and Interface Science*. 1999;80(1):27-50.
23. Butt HJ, Graf K, Kappl M. *Physics and Chemistry of Interfaces*. Weinheim, Germany: Wiley-VCH Verlag GmbH & Co. KGaA; 2003.
24. Gualda GAR, Ghiorso MS. Magnetite scavenging and the buoyancy of bubbles in magmas. Part 2: Energetics of crystal-bubble attachment in magmas. *Contributions to Mineralogy and Petrology*. 2007;154(4):479-90.
25. Lopez-Sanchez M. GrainSizeTools: a Python script for grain size analysis and paleopiezometry based on grain size. *The Journal of Open Source Software*. 2018;3:863.
26. Saltikov SA, editor *The Determination of the Size Distribution of Particles in an Opaque Material from a Measurement of the Size Distribution of Their Sections*. *Stereology*; 1967 1967//; Berlin, Heidelberg: Springer Berlin Heidelberg.
27. Edmonds M, Brett A, Herd RA, Humphreys MCS, Woods A. Magnetite-bubble aggregates at mixing interfaces in andesite magma bodies. *Geological Society, London, Special Publications*. 2015;410(1):95.
28. Fiege J, Webster J, Simon A, Holtz F. Accumulation of magnetite by flotation on bubbles during decompression of silicate magma. *Scientific Reports*. 2019;9.

FIGURE CAPTIONS

SUPPLEMENTARY FIGURES

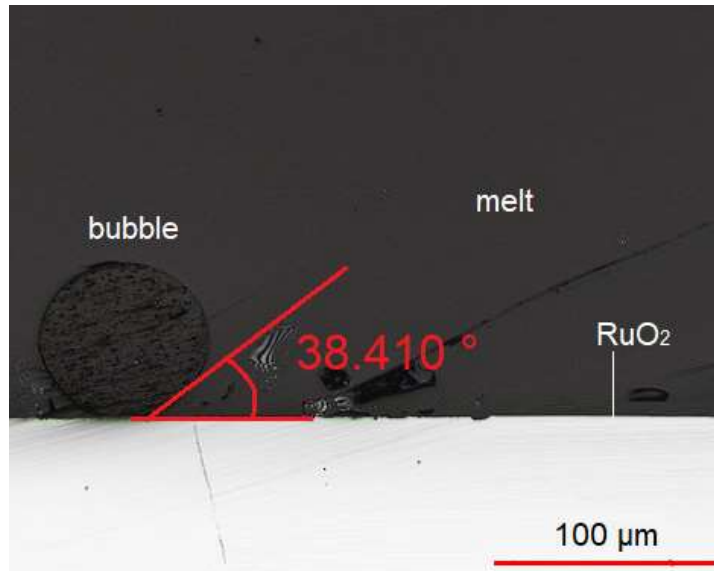


Figure S1: Example of a measurement of contact angle (Ψ) between bubble-RuO₂ immersed in the borosilicate melt.

The average value of 10 measurements is $\Psi = 41.4 \pm 3.5^\circ$. Bubble texture is due to epoxy filling and polishing.